Bent out of shape: Bioinspired vertebral column morphology and mechanics

Cassandra M Donatelli[1] and Dr. Marianne E Porter[2]

Blinks Research Fellowship 2013
Summer 2013

[1] University of Rochester
[2] Florida Atlantic University

Contact Information
Cassandra M Donatelli
University of Rochester
500 Joseph C. Wilson Bvld.
CPU 271286
cdonatel@u.rochester.edu

Keywords: Biomechanics, Vertebrae, Centra, Swimming, Biomimetic, Bioinspired

Abstract

The vertebral column plays an essential role in body stiffness and swimming. Greater body stiffness results in greater mechanical outputs from the body on the environment. Previous work in bioinspired systems has shown that changing the length of the intervertebral joint changes the mechanics of the whole column. Our goals were to test the effects of centrum morphology and intervertebral joint length on mechanical outputs of the vertebral column using bioinspired models. We expected that centrum angle, joint length, and bending angle would all be significant effects in our statistical models. We designed five 3-D models inspired by vertebral morphology of fishes, humans, and marine mammals, and models were printed on a 3-D printer. We constructed 12 motion segments (centrum – joint – centrum) of varying joint length for each centrum morphology. A moment arm was added to one end of the motion segment to insure pure bending and eliminate shear. We tested mechanical properties of motion segments on a materials testing system measuring force (N). From the force outputs we calculated moment (Nm), Work (J), and Bending Stiffness (Nm2). Increasing the bending angle during testing, increased the moment and work produced by the system, while it decreased the bending stiffness. By increasing joint length we measured decreases in each of those mechanical properties. The marine marine mammal models, regardless of joint length, always had the largest mechanical outputs while the fish model with an intermediate centrum angle had the lowest. These data suggest that convex and flat models are consistently stiffer than concave models. Our data show the relation between centrum shape, joint length, and their associated mechanical outputs is perhaps not linear. Building additional models will allow us to further explore morphospace and better understand the conserved centrum shapes we see in among vertebrate groups. This research was funded by NSF grant DBI 1262239.

Introduction

During aquatic locomotion, body stiffness directly affects the external forces needed to reach ideal swimming speeds. The American Eel (*Anguilla rostrata*) uses muscle to triple their body stiffness. Increasing body stiffness decreases the cost of body movement during steady swimming, and also increases net positive muscle work done by the body on the surrounding water (Long 1998). As the fish body pushes against the water, increased external work creates a moving wave of muscle matching the body's natural bending frequency. In engineering, when a beam, which can be compared to the body of the eel, reaches its natural bending frequency, it can flex continuously at the same amplitude throughout its length. For the eel, this principle means that the work needed to swim at this pace is reduced. Conversely, decreasing body stiffness also decreases the net work done on the environment by the fish. Body stiffness in the Longnose Gar (*Lepisosteus osseus*) decreases when skin scales are removed (Long *et al*., 1996). Decreasing body stiffness increases the ideal tail beat amplitude and total power used by the fish to swim at its body's natural bending frequency (Long *et al.*, 1996). Increasing amplitude and power, results in higher energy use by the fish to travel at its ideal speed.

Increasing vertebral column stiffness has a significant effect on a number of mechanical properties that play a role in swimming. Increasing the number of vertebra per unit length increases stiffness in a bioinspired column. As stiffness increases, several mechanical properties also increase such as storage modulus (E'), loss modulus (E''), peak acceleration, and mean speed (Long *et al* 2011). Knowing these internal mechanical properties, the structure of the vertebral column can be inferred by measuring external properties such as bending angle externally during a turn. For example, the second moment of area (m^4) of the vertebral centra is an important factor predicting body curvature (Porter *et al.*, 2009). Spring stiffness (N/m) of the

vertebral column is proportional to the ratio of the second moment of area in the centra (related to centra radius) and the centra length (Porter *et al.,* 2009). Our goals are to look at the effect of centra depth and angle on the stiffness of the vertebral column.

In addition to the vertebrae, intervertebral joint (IVJ) morphology can also impact the stiffness of the whole vertebral column. The intervertebral joint is comprised of several structures. The vertical septum, external connective tissue, is essential for keeping the column intact; however, it has little effect on the stiffness (Nowroozi and Brainerd 2012). The encapsulating tissue (including the elastic externa, external intervertebral ligament, and fibrous sheath) surrounds the IVJ and connects to the adjacent centra cup edges. This plays a crucial role, and when it is cut, the stiffness of the joint drops drastically (Nowroozi and Brainerd 2012). As the stiffness of the IVJ increases, the required work by the muscle to bend them increases (Long, 1992). Increasing stiffness of the IVJ causes an increase in the bending moment of the vertebral column as a whole (Long, 1992).

In swimming robots, changing the morphology of the biomimetic vertebral column causes changes in the swimming speed and frequency (tail beats per second). Several aquatic robots have been built using biomimetic vertebral columns such as Tadro4 and MARMT (Long *et al.,* 2011). Data from these robots suggests that in biological systems, centra morphology affects the overall performance of the vertebral column when it is used as a propulsive tail. For example, IVJ length plays a large role in spinal mechanics. When intervertebral joints are small, the storage and loss moduli are large, resulting in overall greater stiffness. When E values (Young's Modulus) are larger, more work is required to bend the column, but that work is then stored as potential energy and released onto the external environment during every tail beat (Long *et al* 2011). Biomimetic models are powerful tools when looking at mechanical properties

because they allow us to explore a wide range of morphospace, differing shapes and arrangements, which would not be possible in biological systems.

Our goal is to explore a wider range of the morphospace by examining the role of centra angle and IVJ length on the mechanical outputs of one motion segment: a centrum – IVJ – centrum system. Previous work on vertebral column morphology and mechanical outputs has been done on a variety of species, but it can be difficult to compare morphological differences across species due to differences in skeletal building (bone and cartilage) and IVJ materials. Biomimetic models are way to compare morphology of the vertebrae and IVJ's without having to account for material composition and structure. In this study, motion segments were inspired from the Bonnethead shark (*Sphryna tiburo*), Blacktip Shark (*Carcharinus limbatus*), Spiny Dogfish (*Squalus acanthias*), California Sea Lion (*Zalophus californiacus*), Grey Whale (*Eschrichtius robustus*), and Humans (*Homo sapien*), encompassing both fish and mammals. We hypothesized; as concavity of the centra increases that resulting forces would decrease due to larger volume of IVJ material resulting in decreased reaction forces against solid centra model. Also, as IVJ length increases, we hypothesized resulting forces due to bending of the motion segment will decrease. Finally, as applied bending angle increases, we expect required forces generated by the motion segment to increase.

Methods

3D Models and Printing

The 3D centra models were created with the program Google SketchUp. Three of the models are based off of fish centra. In Long et al (2011), the three bioinspired fish models were based on measurements of Bonnethead (*Sphryna Tiburo*) and Blacktip (*Carcharinus limbatus*)

shark vertebra (Table 1). The three centra cone angles they use are 90 º, 120 º, and 150º. In addition, we measured vertebrae from a spiny dogfish (*Squalus acanthias*), and found the angle of its centra to be 101º. For comparative purposes, we designed our models similar to those in Long *et al.* (2011). We scaled models appropriately to fit in our testing systems. The angles we used were 87.76 º, 118.10 º, and 148.70º for the fish models (Fig. 1). For naming convention purposes, we will call them 90 º, 120 º, and 150º. The fourth and fifth models were based on terrestrial and marine mammals. The terrestrial model is flat (180º), causing the IVJ to be a flat disc, as in humans. The aquatic mammal model has an outward protrusion measuring 211.30º (called 210 º here after). This model was based on measurements taken from Grey Whale and Sea Lion vertebrae at The Whale Museum at Friday Harbor (Fig. 2). All of the centra models were 30mm high at the perimeter and had a diameter of 25mm. The centrum cup was added at one end of the model while the other ends were used to attach a moment arm to the end of the motion segment and to be mounted in the bending rig (Fig. 3). Once the models were drawn in SketchUp, they were exported to universal .stl file format, a standard file type, used by a variety of 3D printers and programs.

We printed models on a ZCorporation ZPrinter 310 using High Performance Composite Powder and adhesive for binding (Fig. 4). Immediately after printing, the models are soft and easily damaged. We solidified models by spraying them with an epsom salt solution, hardening the models while still allowing them to be porous. The porous surface was better for binding with the silicone used as the IVJ material. On the ZPrinter, up to 30 of centra models were printed in one batch. ZPrinter models are nearly identical to the SketchUp files. The models are smooth and consistent in their shape and fill density allowing us to assume constant material properties of the model in our calculations.

We built motion segments by placing two centra models in a PVC tube marked with the desired IVJ length (Fig. 5). The gap, IVJ, was filled with 3M marine grade silicone. Through the curing process, the silicone expanded the length of the IVJ. As a result, the IVJ lengths varied among motion segments, and were analyzed as a continuous variable. The individual motion segments cured in the PVC for three days before being removed. Motion segments were allowed to air dry for an additional three days. After that, a ¼" diameter, steel moment arm was added to one end of the segments and secured with cyanoacrylate and an accelerator spray. The hole in the centrum model was 6.5mm in diameter and was included in SketchUp so it was incorporated during 3D printing. Moment arm length ranged from 11.5 to 13cm and was inserted 1cm into the motion segment. To assure a consistent moment arm length, the moment arm was marked at 10cm from the free end of the model.

Mechanical Testing

Each motion segment was inserted and secured with a screw into a bending rig with a set height of 26.0cm and insertion depth of 1.7cm (Fig. 3). The moment arm was positioned under the motion head of the MTS Synergie100 test system (MTS, Eden Prairie, MN, USA) with a 10 N load cell. The addition of the arm was necessary to create a bending moment at the IVJ, rather than pull the end of the segment and shear it. To allow for bending, and avoid shear, we used a wire to pull the moment arm rather than having the motion head on the MTS grip the arm directly (Fig. 4). The wire was placed 10 cm from the proximal centrum at the end of the moment arm. Without the wire, the MTS pulls the motion segment straight up causing shear, rather than allowing it to rotate and create a moment. The wire allowed the moment arm to rotate as it was being pulled, eliminating shear. In addition, the bending rig was secured to the

table with clamps to keep its position relative to the MTS standard.

We controlled the MTS and collected data using TestWorks. We designed a method to extend the height the actuator head to measure bending in the motion segment. The TestWorks method has several steps. First, we pre-load the motion segment with 0.1 N to ensure any slack is pulled out of the wire. After the pre-load, the MTS pulls the moment arm to a calculated height for bending the IVJ at four specified angles, 1º, 2º, 3º, and 4º. The motion segment is measured prior to every test to determine the height in mm (H) the MTS will have to travel to reach the desired angle in degrees (θ) (Equation 1) (Fig. 6).

Equation 1.

where:

Lastly, the MTS returns the wire and moment arm to a height of 0mm. This is repeated 5 times with a speed of 100mm/min and a data collection speed of 100hz.

Calculations

The raw data from the MTS was collected at 100 hz and gave us displacement of the motion head and the resulting force. All of our mechanical data were calculated using our measurements, and these results. First, the average peak load was taken from the peaks of the five cycles done per test. Once we found average load, several other mechanical properties could be calculated.

The first property calculated was Moment (N). Moment was calculated using:

Equation 2:

Where M is the moment, F is the force required to bend the joint at the specified angle, and MA is the distance from the center of the IVJ to the location on the moment arm gripped by the wire (Fig. 7).

Work (J) was calculated as:

Equation 3:

Where W is work, F is the force required to bend the joint at the specified angle, and H is the height the motion head travels to create the specified angle between the center of the IVJ and the horizontal.

We also calculated Bending Stiffness ($N*m^2$) as:

Equation 4:

Where EI is bending stiffness, F is the force required to bend the joint at the specified angle, MA is the distance from the center of the IVJ to the point where the MTS gripped the moment arm, and H is the height the motion head travels with the end moment arm.

Once Bending Stiffness was calculated, Young's Modulus (E) could be calculated by dividing by the moment of Inertia. Moment of Inertia is given by:

Equation 4:

Where r is the radius of the cylindrical model. Once E was calculated for each model, the average (E*) was taken.

Storage modulus (E') and loss modulus (E") can be calculated using E* and δ. The time labeled data from the MTS tests are used to measure δ. To get a value, the difference between

the time of the peak extension of the motion head and the peak force is taken. This was done for seven random samples which were bent at 2 degrees and the average was taken to get our δ value. Storage and loss modulus were then calculated using:

Equation 5:

and

Resilience can also be calculated using δ. The equation used was:

Equation 6:

Statistical Analysis

To determine whether or not the results are significant, we used a Regression model. Our variables are Centra Angle, IVJ length, and Degree of Bending. Because all of our variables can be measured, they were treated as continuous variables. The response variables calculated are Average Force, Work, Moment, and Bending Stiffness. JMP was used to generate our p-values, and a Bonferoni correction was used to modify the standard significance value of $p < 0.05$. Because we are using each model 4 times, our p value must be less than 0.0125 to be significant.

Results

Mechanical Properties

The results of the calculation of Moment (Equation 2) were graphed in relation to IVJ length and separated into different panels by degree of bending (Fig. 8). Running a fully-factorial regression model for Moment relating to Centra Angle, IVJ length, and Angle of

Bending showed that the model was significant ($p<0.0001$, adjusted $r^2 = 0.877172$, $F = 260.13_{7,247}$) (Table 3). The results show that moment increases as degree of bending increases. Also, as IVJ increases, moment decreases. As the bending increases, the difference in morphologies becomes more apparent. At 1°, the values for moment range between 0.1 N*m and 0.2 N*m, a difference of 0.1. However, at 4° they range from 0.15 N*m to 0.51 N*m, a difference of 0.35. Though the range changes, the order of the trends stays the same with 210º always having the highest average moment and 120 having the lowest. Moment describes the tendency of a force to rotate an object around a point at the end of a moment arm. Our data suggest that 120 º models tend to rotate more easily and 210º models rotate less.

The results of the Work calculation (Equation 3) were graphed in relation to IVJ length and separated into different panels by degree of bending (Fig. 9). Running a fully-factorial regression model for Work relating to Centra Angle, IVJ length, and Angle of Bending showed that the model was significant ($p<0.0001$, adjusted $r^2 = 0.919843$, $F = 417.4001_{7,247}$) (Table 3). The amount and range of work required to bend the motion segments increases drastically with degree. At 1°, all of the models require less than 0.0035 J to bend. At 4° the maximum work required is 0.035 J, and entire order of magnitude higher then bending at 1°. In general, it takes the most work to bend the 210º motion segment and the least work to bend the 120 degree motion segment.

For Bending Stiffness, the results of the calculation (Equation 4) were graphed in relation to IVJ length and separated into different panels by degree of bending (Fig. 10). Running a fully-factorial regression model for Bending Stiffness relating to Centra Angle, IVJ length, and Angle of Bending showed that the model was significant ($p<0.0001$, adjusted $r^2 = 0.73127$, $F_{7,247} = 99.74$) (Table 3). At one degree, the max Bending Stiffness is with the 180º model around

0.455 N*m^2 while, at 4º, the max is only around 0.325 N*m^2. Though the range changes, the 210º motion segments has a consistently higher Bending Stiffness and the 120º motion segment has a consistently lower Bending Stiffness.

Discussion

Implications for Swimming

The stiffer a body is, the better it is at swimming (Long *et al* 2011, Long 1998, Long 1995, Long 1992, Long *et al* 1990, Nowroozi 2012). In fish, the vertebral column provides structure and support for swimming. We can assume that the stiffer the vertebral column is, the stiffer the fish body will be, and the better it will be able to swim and maneuver through the water. In this case, we would assume that fish would favor centra morphologies that allow their vertebral column to be more stiff. In the blacktip and bonnethead sharks, their centra angles range from 70° to 140° degrees (Long *et al* 2011). In our models, 120° is the least stiff, and stiffness increases at 150°. Stiffness also increases in the opposite direction towards 90°. We would need to test more angles in the "less than 90°" direction to determine whether or not stiffness increases in that direction.

It is important to note that other factors play a role in spinal stiffening such as connective tissue (Nowroozi 2012). Though the angles in nature tend to fall into our "less stiff" category, we need to remember that fish have a range of different centra angles throughout their vertebral column. It could be that the stiffer angles such as 150° or 90° are present in areas needed for motion, such as the tail region, while less stiff angles such as 120° are present more near the head where there are fewer fine swimming maneuvers.

Fishes have been observed to swim in four distinct patterns; Anguilliform Swimming, Subcarangiform swimming, Carangiform swimming, Thunniform swimming (Hebrank 1982). Anguilliform Swimming is used by eels. In Anguilliform Swimming, a wave of bending travels from the head of the fish to the tail. We would expect that it would be important for the body to be consistently stiff throughout the length to allow for this type of swimming. Goldfish use what is called Subcarangiform swimming where the wavelength is not continuous. The wave starts small at the anterior end and increases as it travels to the posterior. Vertebrae morphology, in this case, would allow for less stiff morphologies at head and stiffer morphologies near the tail. In Carangiform swimming, only the last half of the fish's body is involved in the bending motion. In this case, the vertebrae at the tail end would need to be stiffer then the vertebrae at the head. Lastly, Thunniform swimming, named after the Tuna, is where only the peduncle and caudal fin create forward movement. In fish which use this type of swimming, there may be more room for less stiff vertebrae morphologies until the tail joints.

Discussion of Results

Our data supported our hypothesized that moment and work will decrease as IVJ length increases, also moment and work will increase with increases in bending angle (Fig. 8 and 9). Since work takes into account the height traveled of the motion head, along with force, it varies more than the moment. The moment arm length is relatively constant between models, varying by only a small fraction (less than 1%) so changes in moment are driven by the forces measured with each motion segment morphology. Height traveled of the motion head ranges from just over 2mm, up to over 9mm, an increase of over 400%. As a result, work increases by an entire order of magnitude from 1 to 4 degrees.

Bending stiffness decreases as IVJ length increases, but, it decreases with bending angle, rather than increasing (Fig. 10). Instead of measuring the force resulting from bending the motion segment, bending stiffness measures the motion segments resistance to bending. For this reason, it makes sense that bending stiffness decreases with an increase in degree of bending. As the MTS applies more force to the end of the moment arm, the motion segment is less able to resist that force.

There are four possible trends which could be inferred from the effects of centrum morphology on average bending stiffness (Fig. 11). A positive trend in our data (Fig. 11A) would support the hypothesis that resulting forces decrease as centra angle decreases. Also, the 90° model does not fit the trend produced by the rest of the morphologies. This model suggests that the motion segments are stiffer based on centra shape alone. If true, the parabolic trend (Fig. 11B) shows stiffness increasing in both small convex and larger concave angles and with the 120° model as the inflection point of the curve. If stiffness increases at both ends of this parabolic curve, there may be a tradeoff centrum morphology and associated swimming performance. The two hypothetical exponential decay trends (Fig. 11C and D) also support the hypothesis that stiffness decreases with centra angle, but plateaus around either 90° (Fig. 11C) or 120° (Fig. 11D). Similar to the positive trend (Fig. 11A), either the 120° (Fig. 11C) or the 90° (Fig. 11D) models would not fit the exponential decay curve. These models suggest that the motion segment would be less stiff due to 120° (Fig. 11C) or more stiff at 90° (Fig. 11D) based on centra angle. This same thought experiment is true for all mechanical properties examined here.

Biological and Biomimetic Systems

To determine the biological relevance of our models, we compared our results to Nowroozi's work with striped bass (Nowroozi 2012). When scaled up to the size of my models, the average IVJ length of the Striped Bass is about 8mm and the centrum angle is 90º. The max moment from bending striped bass centra at the IVJ is between 0.13 and 0.14 N*m. If we also examine moment from bioinspired motion segments at 8mm IVJ, the only 0.13-0.14 N*m outputs occur during 2º bending and also in the 90º model. Our models are biologically relevant.

Biomimetic vertebral columns have been used to test other mechanical properties such as Storage and Loss Modulus (E' and E"). In previous models, both E' and E have been shown to decrease as IVJ increases. Our data show the same trend (Fig. 12).

Further work

To test the trend related to decreasing centra angle, we would like to make several models at degrees less than 90° such as 75°, 60° and 45°. We would also like to determine if the nature of the valley around 120° by creating more concave models between 90° and 150° at 15° increments (90°, 105°, 120°, 135°, 150°). We would also love to make several convex models to test the trend in the positive direction after 210°.

Another interesting thing would be to look at different IVJ material. The silicone we used is relatively stiff for an IVJ material. It would be good to look at how different materials interact with our different centra shapes.

Acknowledgements

We would like to thanks to Adam Summers and Sophie George for writing the grant to fund this research, Vik Iyengar and Scott Schwinge for organizing the program, everyone in FHL's Lab 8

for allowing me to use their space to work, Rachel Merz and her lab interns for help and support, Adrienne Dunk for providing baseline data for the project, the Whale Museum at Friday Harbor for allowing me to photograph and measure their marine mammal vertebrae, Friday Harbor Labs staff and faculty, and the Blinks/NSF REU/BEACON Program.

Tables

Table 1

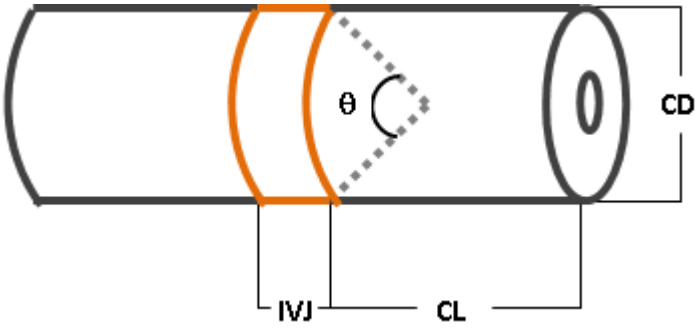

Model		Centra Length (CL) (mm)	IVJ Length (IVJ) (mm)	Centra Diameter (CD) (mm)	Centra Cone Angle (θ) (degrees)
Bonnethead (*Sphryna tiburo*) (Long et al 2011)	Actual Values	11	2.8	10	90, 120, 150
	Scaled Values	27.5	7	25	
Blacktip (*Carcharinus limbatus*) (Long et al 2011)	Actual Values	6	1.3	8	
	Scaled Values	18.75	4.06	25	
Dogfish (*Squalus acanthias*)	Actual Values	~ 3.8	~0.57	~4.43	~100
	Scaled Values	21.432	3.21	25	
Bioinspired Motion Segments		30	6, 7, 10, 13	25	90, 120, 150, 180, 210

Table 1. Bioinspiration for the models used in this study. Measurements reported in Long et al. (2011) were from the maximum values found in the Bonnethead and Blacktip sharks. The Centra Cone angles presented from Long et al were the values they chose to use in their biomimetic models. We measured the dogfish morphology from a dissection of a fresh specimen.

Table 2

Model	E' (MPa)	E" (MPa)	Material	δ	Resilience
Silicone	9.153	0.3598	**Silicone**	0.0393	0.883837
MARMT (max) (Long *et al* 2011)	0.825	0.1275	**Bone (Curry 2002)**	0.0996	0.730403
Blacktip (max) (Long *et al* 2011)	1.35	0.14	**Cartilage (Curry 2002)**	0.010	0.969072
Bonnethead (max) (Long *et al* 2011)	0.55	0.045			

Table 2. Mechanical properties calculated from our data. Average Storage Modulus (E') and Loss modulus (E") were calculated using E* and Equation 5. Resilience was calculated (Equation 6) using the δ value calculated from 7 random data sets from the MTS.

Table 3

Effect	p Values			
	Average Force	Moment	Work	Bending Stiffness
Entire Model	< 0.0001	< 0.0001	< 0.0001	< 0.0001
Centra angle	< 0.0001	< 0.0001	< 0.0001	< 0.0001
Degree of Bending	< 0.0001	< 0.0001	< 0.0001	< 0.0001
IVJ Length	< 0.0001	< 0.0001	< 0.0001	< 0.0001
Centra angle *Degree of Bending	= 0.0003	< 0.0001	< 0.0001	**= 0.2648**
Centra angle*IVJ length	< 0.0001	= 0.0003	= 0.0002	< 0.0001
IVJ length*Degree of Bending	< 0.0001	< 0.0001	< 0.0001	= 0.0013
Centra angle * Degree of Bending * IVJ length	**= 0.0532**	**= 0.0532**	= 0.0050	**= 0.6905**

Table 3. The significance of our three main mechanical calculations using Degree of Bending, IVJ length, and Centra angle as the three effects. P values were calculated using a regression model in JMP.

Figures

Figure 1

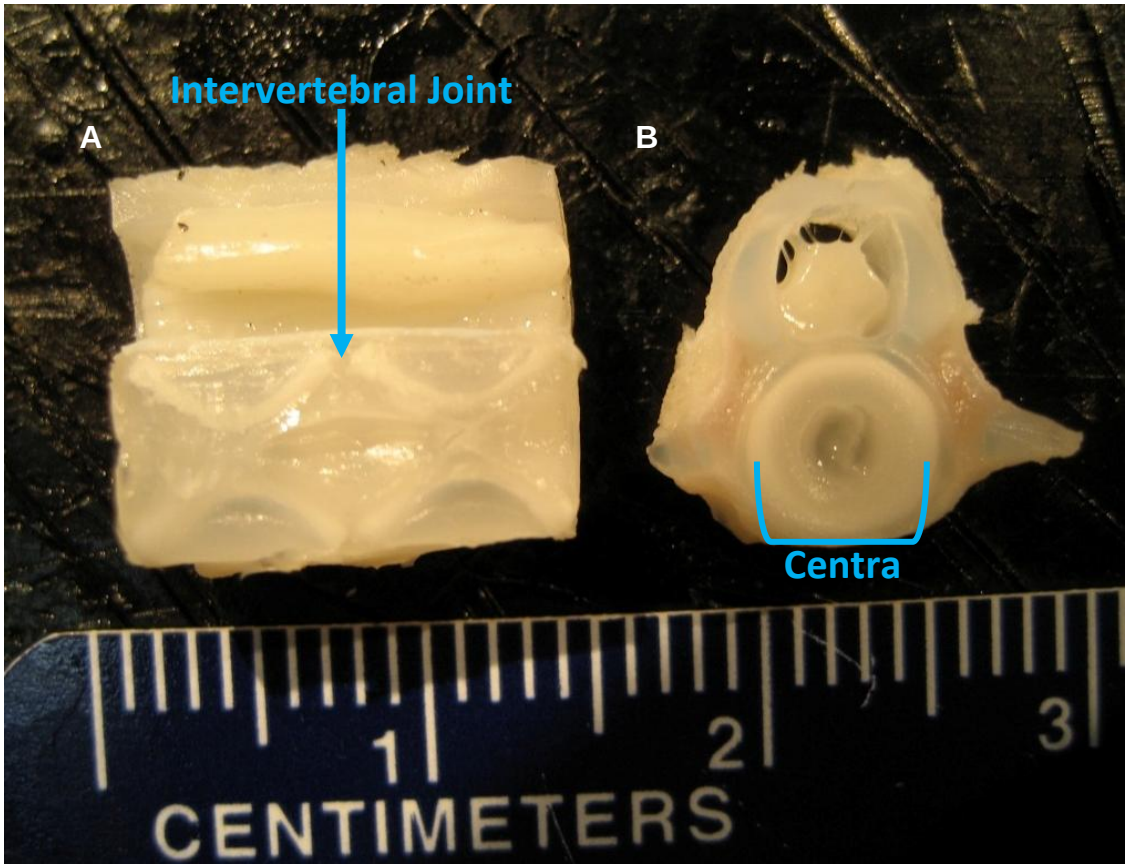

Figure 1. Sagittal (A) and Transverse (B) cut of the Dogfish vertebral column. The mineralized centra and Intervertebral joint are our areas of interest. Also present is the neural arch located above the centra cone in both the Lateral (A) and Anterior (B) view.

Figure 2

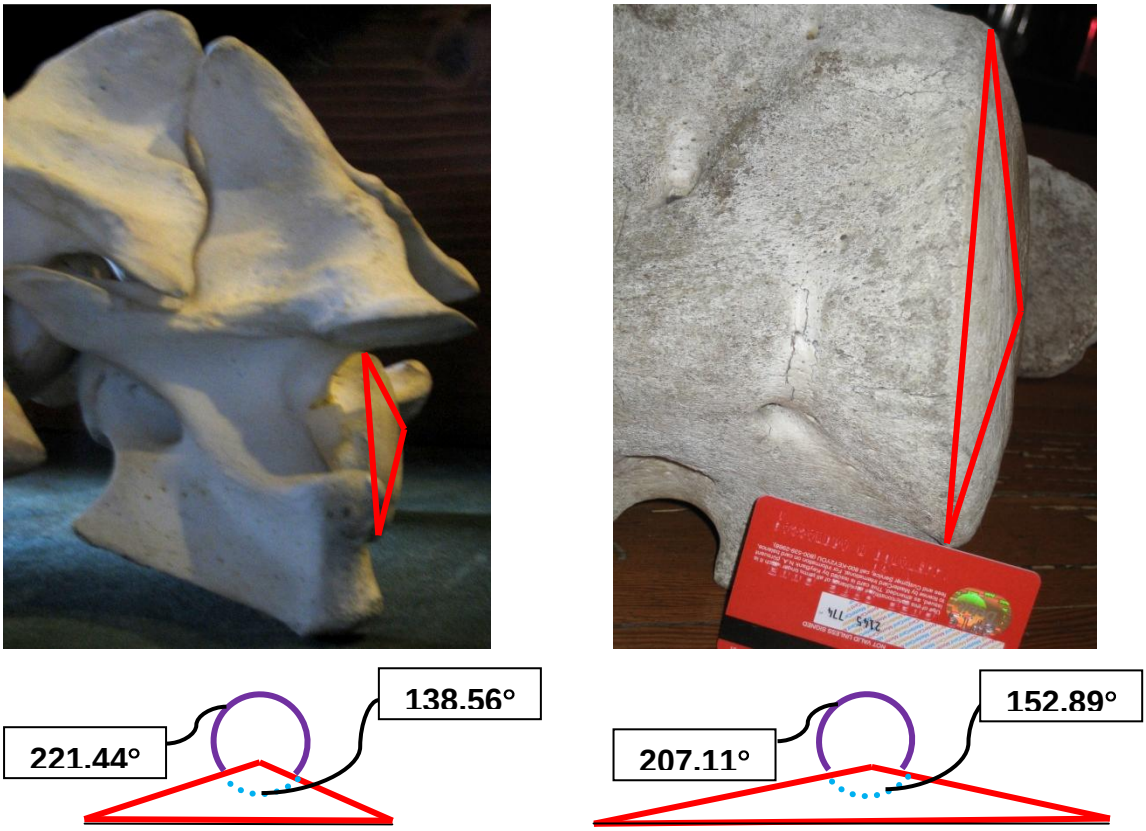

Figure 2: Image of California Sea Lion (Left) and Grey Whale (Right) vertebrae with measurements for use in designing 3D models. Models were traced by hand and angles were calculated.

Figure 3

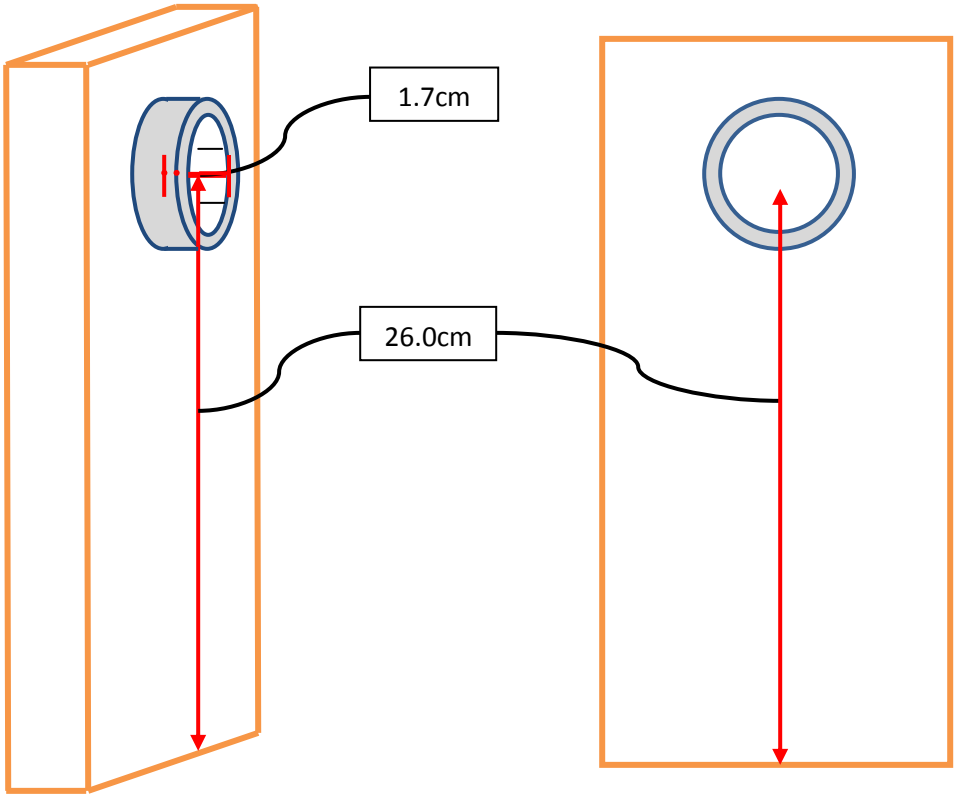

Figure 3: Schematic of testing rig with height and depth measurements.

Figure 4

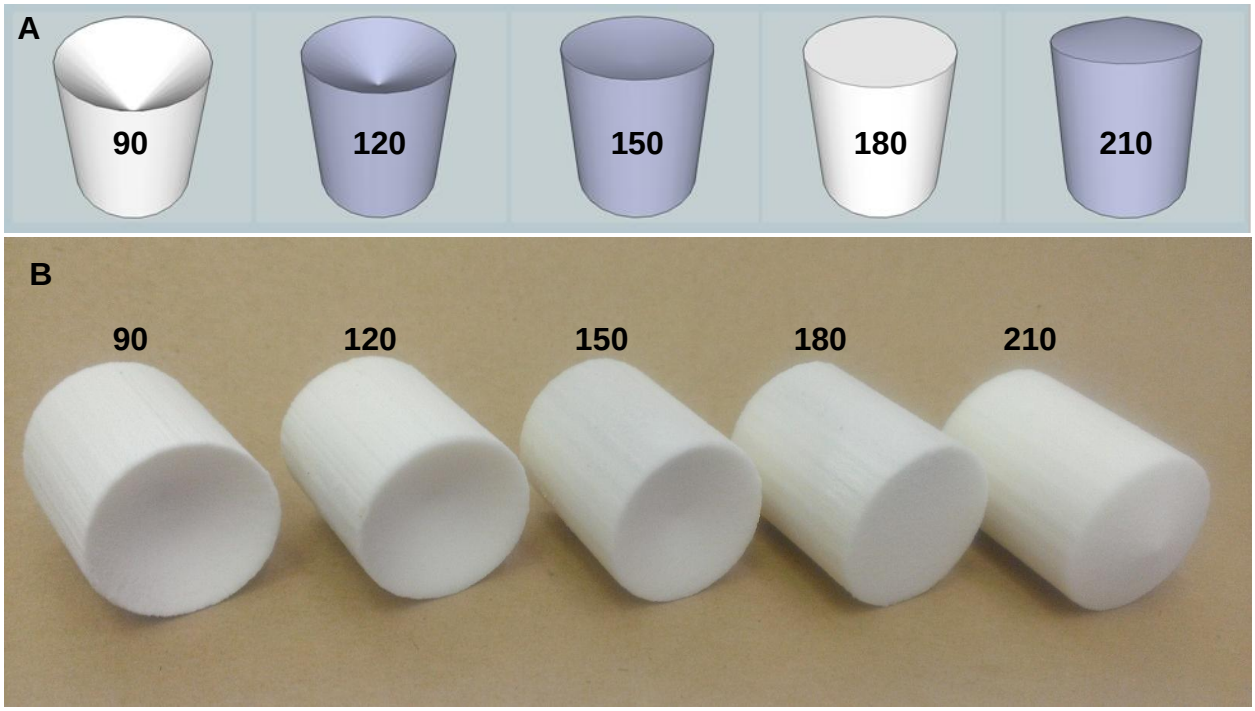

Figure 4. Computer and physical models. These bioinspired models are based on biological morphology reported in **Table 1**. A. SketchUp drawings of bioinspired vertebrae. B. Physical models printed from the Z-Corporation 310 printer following Epsom Salt treatment.

Figure 5

Figure 5: Assembled models. The 6 shown are 180 degree models with various intervertebral joint lengths. The moment arms have been attached with cyanoacrylate.

Figure 6

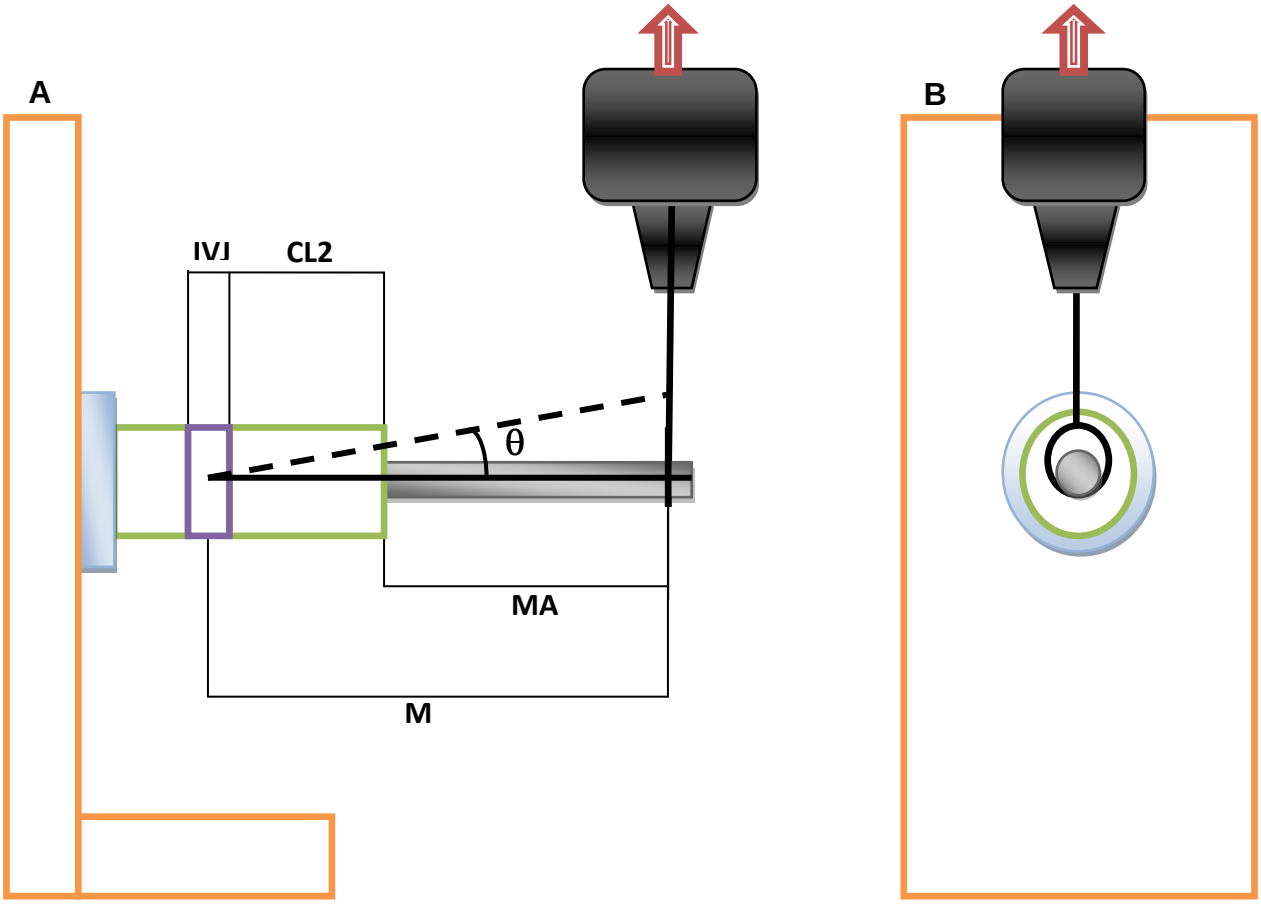

Figure 6. Schematic of the Mechanical testing setup. After calculating the motion head height (Fig. 4), we mounted each motion segment. The motion segment is mounted in the rig with a screw to prevent motion up until the start of the IVJ. In panel A we see a front view with the motion head pulling up on the moment arm of the model. This creates the angle θ calculated using Equation 1. In Panel B we see a side view of the motion head pulling up with a view of the wire looped around the moment arm.

Figure 7

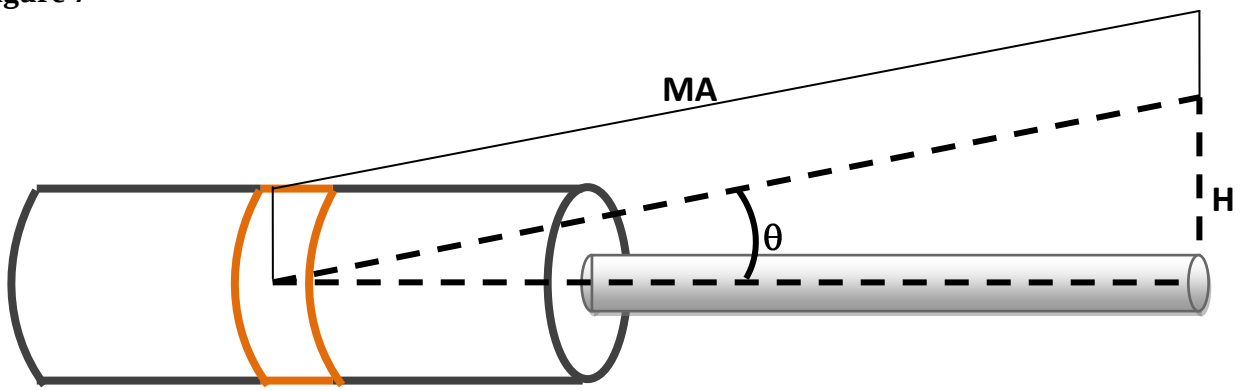

Figure 7. Height (H, mm) of the motion head on the MTS was determined using the moment arm length (MA) and the desired angle of bending (θ) according to **Equation 1**.

Figure 8

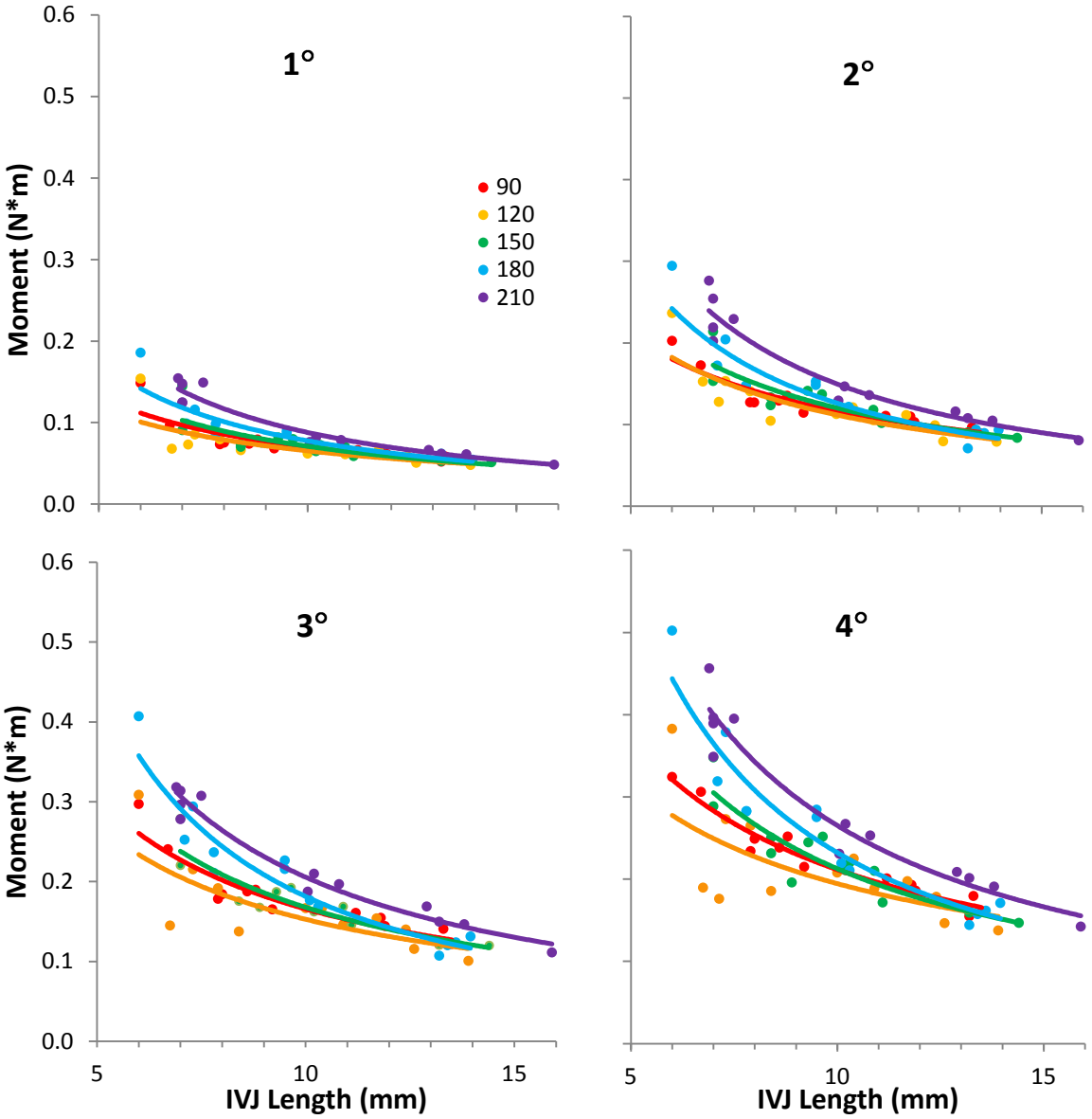

Figure 8. Moment vs. IVJ length per degree of bending. Increasing IVJ length (mm) decreases the moment (Nm) produced. Each panel corresponds to the angle motion segment is bent. Trend lines correspond to each of the 5 centra morphologies tested. A Regression analysis was done in JMP which revealed the model to be significant ($p<0.001$). At each bending angle, the 210º motion segment morphology generates the largest moment, while the 120º motion segment model has the lowest.

Figure 9

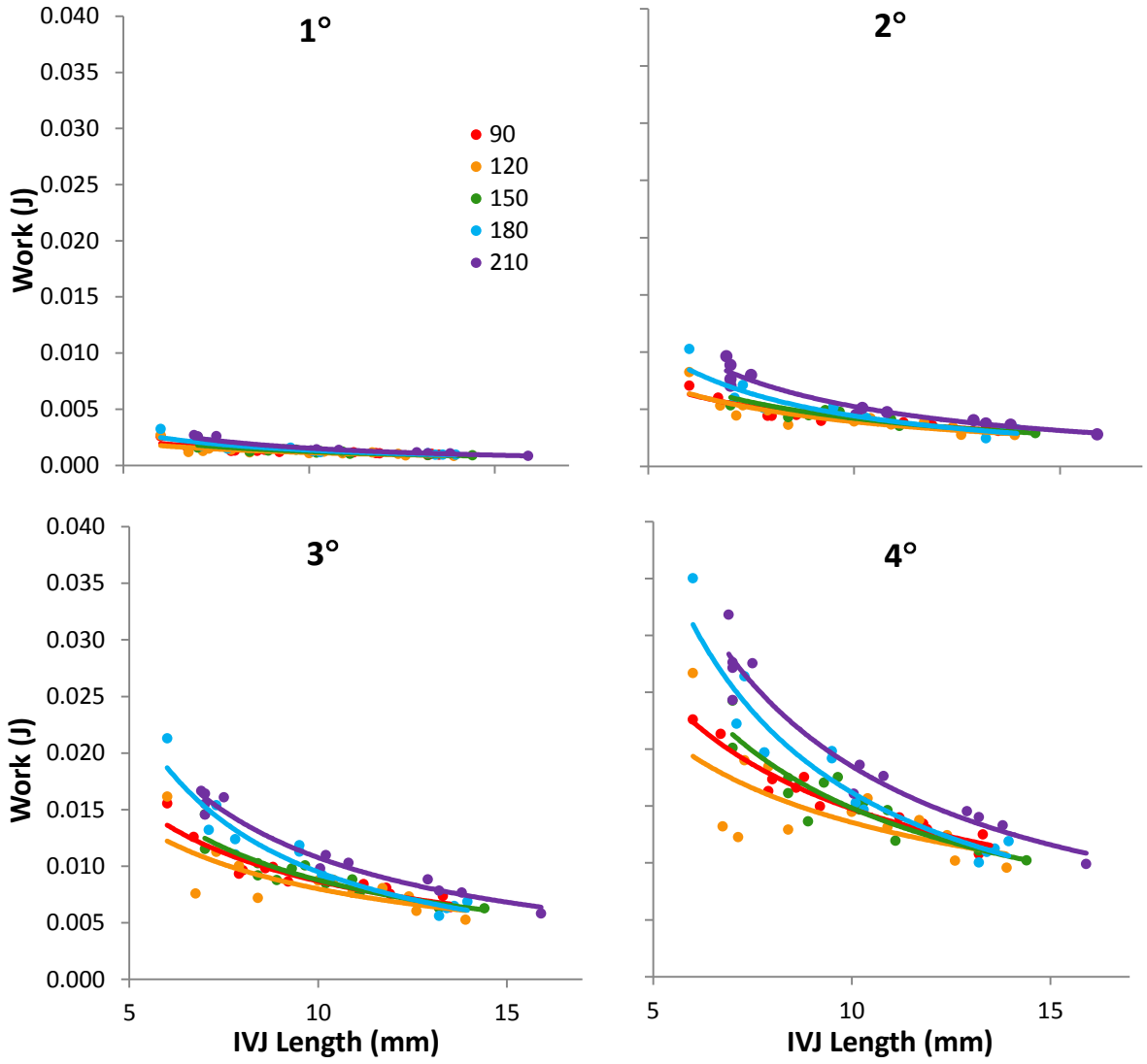

Figure 9. Work vs. IVJ length per Degree of Bending. As IVJ length (mm) increases the Work (J) produced by the motion segment decreases. The panels correspond to the motion segment bending angles. Trend lines are a power fit and correspond to each of the 5 centra morphologies tested. A Regression analysis was done in JMP which revealed the model to be significant ($p<0.001$). For every bending angle, the 210º motion segment models produce the highest average work where the 120º models produce the lowest.

Figure 10

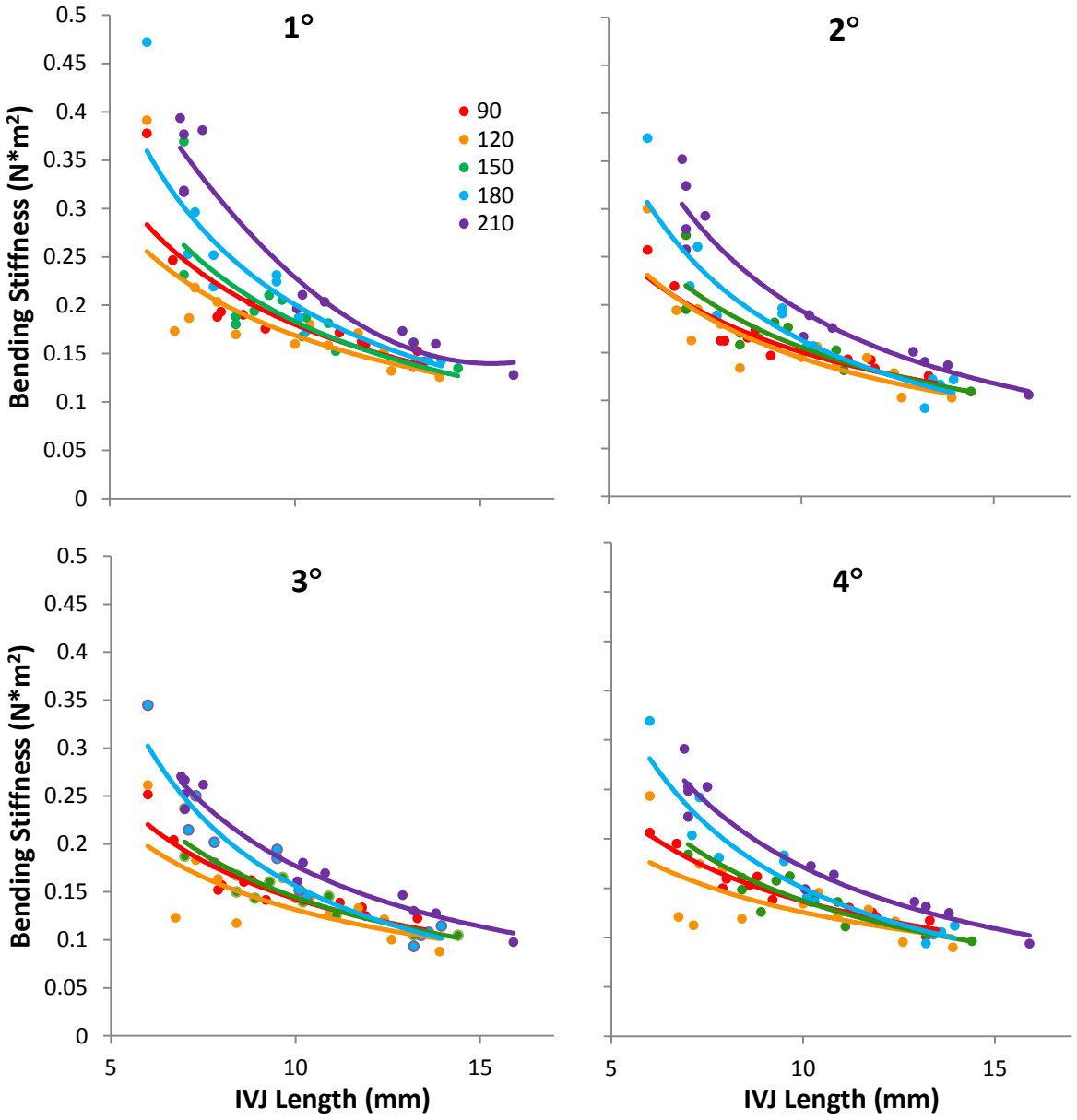

Figure 10. Bending Stiffness vs. IVJ Length per Degree of Bending. Flexural Stiffness ($N*m^2$) decreases with IVJ length (mm). The panels correspond to the motion segments being bent at various angles. Trend lines are power fit and correspond to each of the 5 centra morphologies used. A Regression analysis was done in JMP which revealed the model to be significant ($p<0.001$). For every bending angle, the 210º motion segment model has the highest average flexural stiffness; while the 120º motion segment model has the lowest.

Figure 11 (CHANGE TO BENDING STIFFNESS)

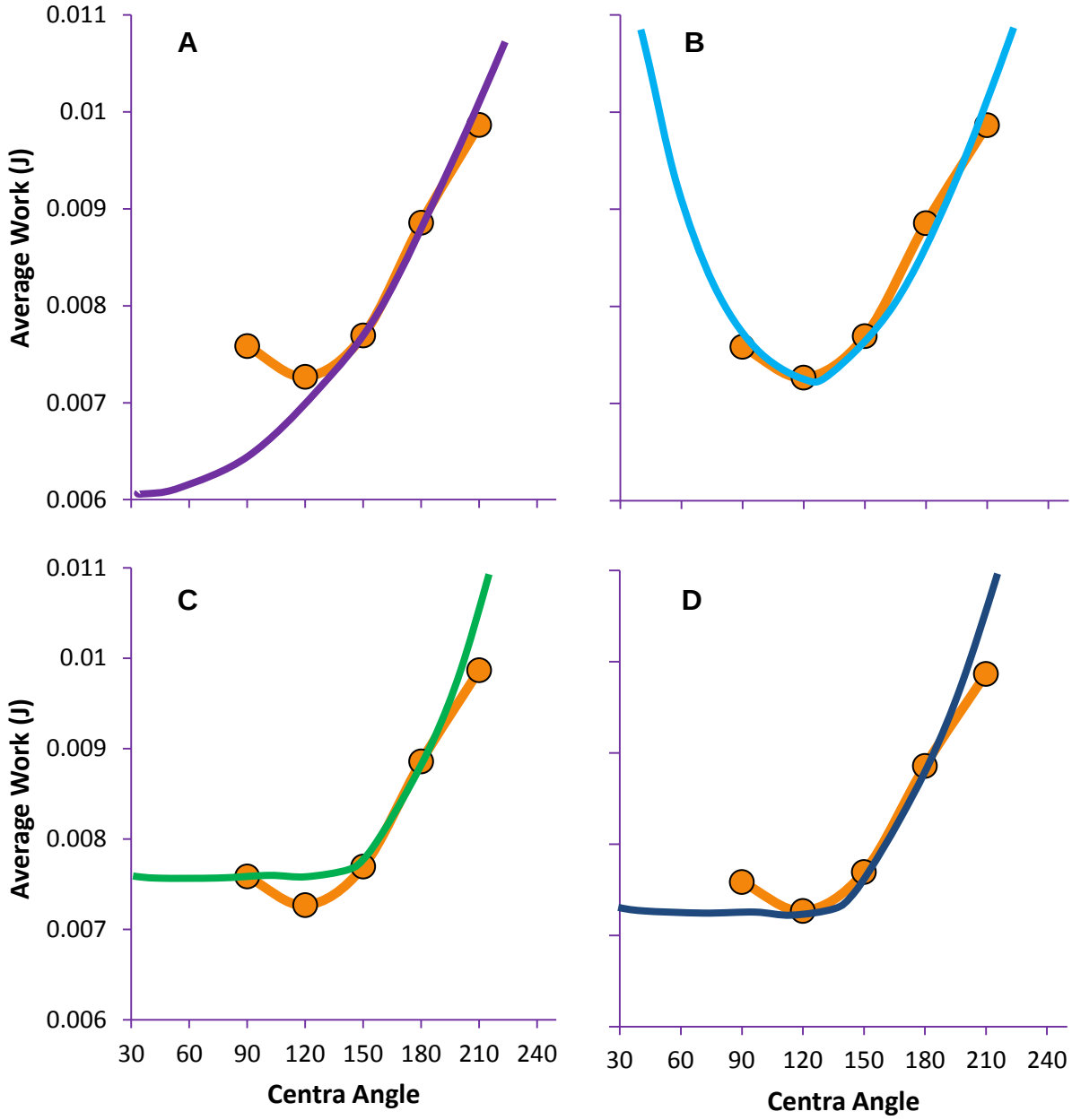

Figure 11. Potential trend lines for further studies. Panel A shows a decaying trend. Panel B shows a parabolic trend line. Panel C shows an exponential trend with the 120 degree model as the anomaly. Panel D shows an exponential trend with the 90 degree model as the anomaly.

Figure 12

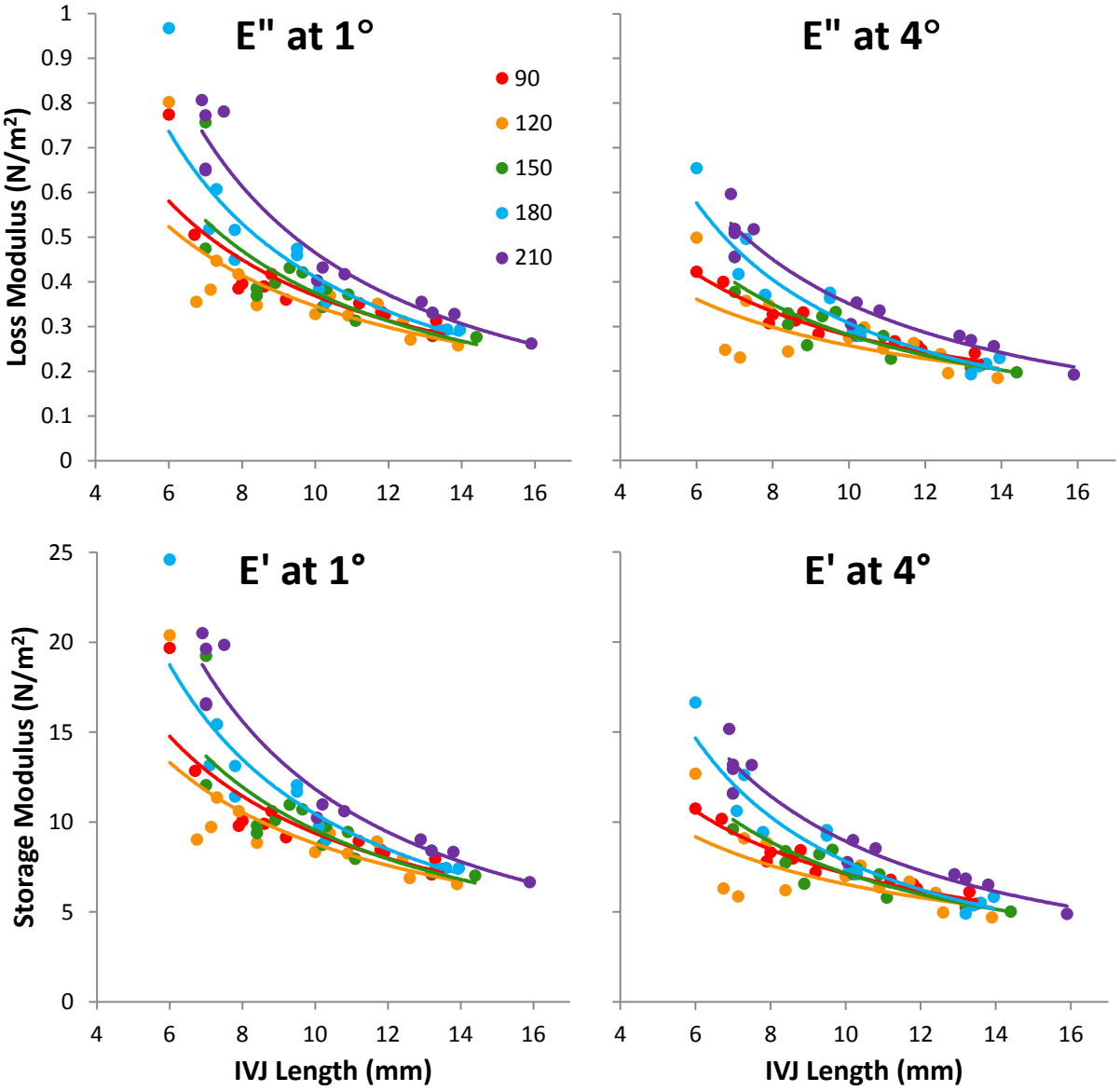

Figure 12. Storage and Loss Modulus plotted against IVJ length. Trend lines correspond to each of the 5 centra morphologies used. Equation 5 was used to calculate these properties.

Literature Cited

Flammang, B. E., & Porter, M. E. (2011). Bioinspiration: applying mechanical design to experimental biology. Integrative and comparative biology, 51(1), 128–32.

Hebrank, J. H., Hebrank, M. R., Long, J. H., Block, B. A., & Wainwright, S. A. (1990). Backbone Mechanics of the Blue Marlin Makaira Nigricans (*Pisces, Istiophoridae*). Journal of Experimental Biology, 459, 449–459.

Hebrank, M. R. (1982). Mechanical properties of fish backbones in lateral bending and in tension. Journal of biomechanics, 15(2), 85–9.

Koob, T. J. (2000). The Vertebrate Body Axis: Evolution and Mechanical Function. Integrative and Comparative Biology, 40(1), 1–18.

Laerm, J. (1976). The development, function, and design of amphicoelous vertebrae in teleost fishes. Zoological Journal of the Linnean Society, 58 (April), 237–254.

Long, B. Y. J. H. (1992). Stiffness and Damping Forces in the Intervertebral Joints of Blue Marlin (*Makaira Nigricans*). Journal of Experimental Biology, 162, 131–155.

Long, J H, Pabst, D. a, Shepherd, W. R., & McLellan, W. a. (1997). Locomotor design of dolphin vertebral columns: bending mechanics and morphology of *Delphinus delphis*. The Journal of experimental biology, 200(Pt 1), 65–81.

Long, John H. (1995). Morphology , mechanics , and locomotion : the relation between the notochord and swimming motions in sturgeon. Environmental Biology of Fishes, 44, 199–211.

Long, J. H., Hale, M. E., McHenry, M. J., & Westneat, M. W. (1996). Functions of Fish Skin: Bending Stiffness and Steady Swimming of Longnose Gar *Lepisosteus Osseus*. Journal of Experimental Biology, 199, 2139–2151.

Long, John H, Krenitsky, N. M., Roberts, S. F., Hirokawa, J., De Leeuw, J., & Porter, M. E. (2011). Testing biomimetic structures in bioinspired robots: how vertebrae control the stiffness of the body and the behavior of fish-like swimmers. Integrative and comparative biology, 51(1), 158–75.

Long, John H. (1998). Muscles, Elastic Energy, and the Dynamics of Body Stiffness in Swimming Eels. Integrative and Comparative Biology, 38(4), 771–792.

Long, John H., Koob, T., Schaefer, J., Summers, A., Bantilan, K., Grotmol, S., & Porter, M. (2011). Inspired by Sharks: A Biomimetic Skeleton for the Flapping, Propulsive Tail of an Aquatic Robot. Marine Technology Society Journal, 45(4), 119–129.

Long, John H., & Nipper, K. S. (1996). The Importance of Body Stiffness in Undulatory Propulsion. Integrative and Comparative Biology, 36(6), 678–694.

Nowroozi, B. N., & Brainerd, E. L. (2012). Regional variation in the mechanical properties of the vertebral column during lateral bending in *Morone saxatilis*. Journal of the Royal Society, Interface / the Royal Society, 9(75), 2667–79.

Nowroozi, B. N., & Brainerd, E. L. (2013). X-ray motion analysis of the vertebral column during the startle response in striped bass, *Morone saxatilis*. The Journal of experimental biology, 216(Pt 15), 2833–2842.

Nowroozi, B. N., Harper, C. J., De Kegel, B., Adriaens, D., & Brainerd, E. L. (2012). Regional variation in morphology of vertebral centra and intervertebral joints in striped bass, *Morone saxatilis*. Journal of morphology, 273(4), 441–52.

Porter, M. E., Roque, C. M., & Long, J. H. (2009). Turning maneuvers in sharks: Predicting body curvature from axial morphology. Journal of morphology, 270(8), 954–65.

Summers, A. P., & Long, J. H. (n.d.). Skin and Bones, Sinew and Gristle: The Mechanical Behavior of Fishes' Skeletal Tissue. Mechanics of Fish Tissues (p. 42).

Ward, A. B., & Brainerd, E. L. (2007). Evolution of axial patterning in elongate fishes. Biological Journal of the Linnean Society, 90(1), 97–116.